Effects of Substrate, Protein Environment, and Proximal Ligand Mutation on Compound I and Compound 0 of Chloroperoxidase†

Wenzhen Lai, Hui Chen, Kyung-Bin Cho, and Sason Shaik*

Institute of Chemistry and The Lise Meitner-Minerva Center for Computational Quantum Chemistry, The Hebrew University of Jerusalem, Givat Ram Campus, 91904 Jerusalem, Israel

Received: March 31, 2009

This paper investigates the enzyme chloroperoxidase (CPO) by means of hybrid quantum mechanical/molecular mechanical (QM/MM) calculations. The effects of anionic substrate, protein environment, and proximal ligand mutation on the high-valent iron−oxo species, compound I (Cpd I), and the ferric hydroperoxide complex, compound 0 (Cpd 0), are studied. The results indicate that the presence of an anionic substrate (acetate) and the protonation state of one critical residue (Glu104) have a considerable impact on the relative stabilities of Cpd I and Cpd 0. In the absence of the substrate or when the substrate is protonated, Cpd I is considerably more stable, and its formation barrier is smaller than in the case where the substrate is in its anionic state and when Glu104 is deprotonated. This trend, which is shown to be a simple manifestation of the Hammond principle, reproduces the experimental observation that the working pH of the enzyme is acidic. Furthermore, in the absence of substrate (or when it is protonated), the relative Cpd 0/Cpd I energies are found to be a good index of Cpd I stability in heme enzymes and to follow the experimental order: horseradish peroxidase (HRP) > CPO > P450. In silico mutation of the proximal ligand from cysteine to selenocysteine was found to have no effect at all on the properties of Cpd I (e.g., spin density on the chalcogen, Mössbauer parameters, etc.) and its relative stability to Cpd 0 or on the corresponding barrier for formation. This surprising finding shows that the polar CPO pocket applies a leveling effect that stabilizes the anionic forms of the proximal ligands ($CysS^-$ and $CysSe^-$). This in turn means that the Se−Cpd I of the mutant CPO is observable.

1. Introduction

Chloroperoxidase (CPO) has received considerable attention because of its outstanding versatility among the known heme enzymes. In addition to its native halogenation and dehalogenation reactions, CPO can catalyze reactions characteristic of classical heme peroxidase, catalase, and cytochrome P450.[1,2] The enzyme has a unique active site that shares features with both peroxidase and P450 enzymes; it contains a proximal cysteine−thiolate ligand as P450 and, at the same time, has a polar distal pocket, as in peroxidases. This polarity of the pocket may account for its versatile function. Moreover, CPO is the only thiolate-ligated heme enzyme, whose oxoiron(IV)−porphyrin cation radical active species, termed compound I (Cpd I), has been well-characterized by various spectroscopic methods,[3−5] thus providing key insight into the behavior of P450s where this species is elusive.[6,7]

Like other peroxidases, CPO Cpd I is generated by the reaction of the enzyme with hydrogen peroxide. By analogy with the distal histidine residue in the plant peroxidases, in CPO Glu183 is postulated to act in an acid−base catalysis of the formation of Cpd I, starting from the hydrogen peroxide complex.[8] It was proposed that Glu183 plays the double role of both proton acceptor and donor during the generation of the catalytically active species Cpd I.[9] In other words, Glu183 is thought to act as a shuttle that delivers the proton of the proximal O atom of the Fe−HOOH complex to the distal O atom, so as to facilitate heterolytic cleavage of the O−O bond (see Scheme 1), in a similar fashion to the Poulos−Kraut mechanism for Cpd I formation in peroxidases.[10] This mechanistic proposal has later been supported by MD simulations[11] and recently by quantum mechanical/molecular mechanical (QM/MM) calculations,[12] which showed that Glu183 initially deprotonates the ferric hydrogen peroxide to yield a ferric hydroperoxide species, called compound 0 (Cpd 0), followed by the generation of Cpd I in a mechanism that involves O−O bond cleavage and reprotonation of the departing OH moiety to water by means of proton coupled electron transfer (PCET).

SCHEME 1: Schematic Mechanism for CPO Cpd I Formation from Ferric Hydrogen Peroxide (Fe−HOOH) via Cpd 0

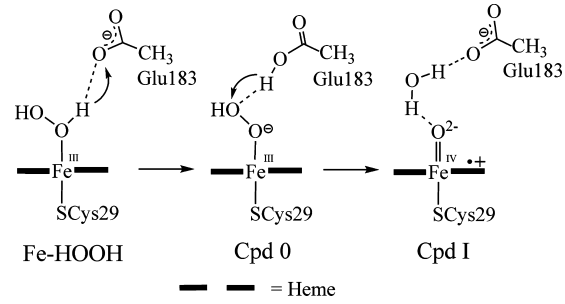

However, this previous QM/MM study[12] showed that Cpd I is merely 1.5 kcal/mol more stable than Cpd 0. Using the relative energy of Cpd 0/Cpd I as an index of the stability of Cpd I and recalling that, for P450cam, QM/MM calculations lead to a reaction exothermicity of about 8 kcal/mol (from Asp251 channel),[13] one is led to a puzzle: this result is counterintuitive, since Cpd I of CPO can be probed in the native cycle, whereas Cpd I of P450cam is still elusive.

Alerted by this puzzling result, we have decided to revisit the problem and find the root cause of the apparent counterin-

† Part of the "Walter Thiel Festschrift".

* Corresponding author. E-mail: sason@yfaat.ch.huji.ac.il.

10.1021/jp902898s CCC: $40.75 © 2009 American Chemical Society
Published on Web 07/02/2009

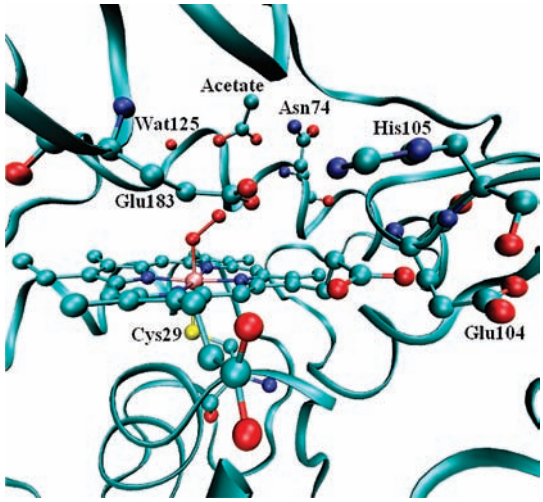

Figure 1. Active site of CPO from the X-ray structure of Cpd 0 (Protein Data Bank code 2J5M).

tuitive result. As shown from the X-ray structure of the ferric hydroperoxide (Cpd 0) complex of CPO in Figure 1,[14] the active site contains an acetate nestled above the heme, at a distance of ~7.0 Å to the heme iron. This acetate forms hydrogen bonds with the amide group of Asn74 (distance: 2.7 Å) and the crystal water molecule Wat125 (distance: 3.7 Å). In fact, the same site was identified as a binding site of acetate in a CPO ferric complex (which contained a Fe−OAc coordination and an acetate bound to Asn74).[15] This site is also known to be the iodide-specific binding site and is thought to act as an intermediate stopping station before the oxidative process.[15] Thus, the acetate anion that was included in our previous calculation[12] in fact is bound in the substrate binding site of CPO, and as such the acetate may have modified the stability of Cpd I. This brings us to one of the central questions of this study: does the substrate affect the stability of Cpd I?

Substrate effects have been reported for P450cam, where it was found out that the substrate can modify the structure and reactivity of the enzyme active site in the early stages of the mono-oxygenase catalytic cycle, that is, the ferric, ferrous, and oxyferrous states.[16−20] Recently, the influence of the presence of substrate on the properties of the active-oxygen heme intermediates was also probed using cryoreduction electron paramagnetic resonance/electron−nuclear double resonance (EPR/ENDOR) by Hoffman et al.[21] It was found that substrates of different sizes dramatically affected the lifetime of Cpd 0. Thus, in the absence of the substrate (camphor) the lifetime of Cpd 0 was extremely short,[21a] while in the presence of camphor derivatives of increasing size, the lifetime increased by as much as 80-fold.[21b] As such, substrates are not just oxidizable entities; they also gauge the lifetime of the active oxidant species. Since acetate was present in our previous study[12] in the substrate binding site, we decide to explore its effect on the stability of Cpd 0/Cpd I by including it in the MM part in different protonation states, that is, deprotonated and protonated acetate, as well as in the absence of acetate.

Another factor that can affect the relative stability of Cpd 0/Cpd I is the nature of the proximal ligand that can be mutated in silico. Thus, our recent work[22] on the selenocysteine mutant of P450cam, in which the cysteinate ligand was replaced by selenocysteinate, postulated that the Se−Cpd I will be formed faster and consumed more slowly than the wild-type (WT) S−Cpd I, thus suggesting that P450 Se−Cpd I would have more chances of being observed than WT species.[23] Recent expression of CPO in *Aspergillus niger*, which enabled mutations of this enzyme and follow-up of its epoxidation activity by Cpd I,[8] suggests that such a C29Se−C mutation may be possible also in CPO and may thereby allow it to further probe factors that stabilize the unstable and highly active Cpd I species. As such, we decided to explore also the role of mutation of Cys29 to Se-Cys in CPO, as part of our attempt to understand factors that affect the stability of Cpd I.

In summary, the main goal of the present paper is to clarify what factors influence the stability of CPO Cpd I. To this end, we gauged the impact of QM regions, protonation states, different enzyme conformations obtained from a molecular dynamics (MD) trajectory, and Cys mutation to Se-Cys. The study was limited to the doublet state that was shown to be the ground state of Cpd I and Cpd 0 by experiment[3] and previous QM/MM study.[12]

2. Computational Methodology

2.1. Setup of the System. An initial geometry was built from the X-ray structure with the Protein Data Bank (PDB) code 2J5M.[14] The glycosyl groups were removed. The complete model of solvated enzyme was constructed by adding missing hydrogen atoms and a 16 Å thick water solvent layer. The inner layer (<8 Å) was equilibrated for 3 ps at 300 K with CHARMM MD. The resulting structure was used as one starting point (snapshot 0) of the QM/MM calculations. For this snapshot no MM minimization was done on the enzyme itself before QM/MM calculations, and thus the coordinates of enzyme heavy atoms correspond exactly to those in the PDB file. The details of the preparatory force field calculations are as described in our previous study.[12]

2.2. Protonation States. ***Prot1 Model.*** On the basis of the pK_a calculation with the PROPKA program[24,25] as well as further visual inspection of the hydrogen-bonding environment of the residues under pH = 3.9 (a working pH of CPO), a neutral protonation scheme, labeled as Prot1, was created. The following residues in Prot1 were protonated: Asp123, Asp149, Asp168, Glu1, Glu51, Glu69, Glu80, Glu99, Glu104, Glu133, Glu155, Glu161, Glu166, Glu201, Glu233, and Glu266. All of the other Glu and Asp residues were ionized; Arg and Lys residues were used as positively charged (Arg26, Arg46, Arg50, Arg111, Arg128, Arg157, Arg160, Arg206, Arg232, Lys112, Lys115, Lys145, Lys177, and Lys211). One His residue (His107) was singly protonated at the imidazole N^{δ} position, and all of the others were doubly protonated. The propionate side chains of heme were ionized. The total charge of the enzyme in Prot1 is 0, in the absence of substrate acetate or in the presence of neutral acetic acid, and −1 in the presence of the acetate anion.

Prot2 Model. The acidic amino acid residue (Glu104, see Figure 1) near the heme center is predicted by PROPKA to be on the border between being protonated and deprotonated (pK_a = 4.8). Thus, a second protonation scheme (Prot2) was created, in which all titratable residues are the same as in Prot1 except for Glu104, which is deprotonated. The total charge of the enzyme in Prot2 is −1 in the absence of substrate acetate.

Prot3 Model. The third protonation scheme, labeled as Prot3, corresponds to the protonation states used in our previous study,[12] in which all of the Glu and Asp residues were deprotonated, all Arg and Lys residues were used as positively charged, and all His residues were doubly protonated. The propionate side chains of heme were ionized. The total charge of the enzyme system in Prot3 is −15 in the absence of acetate or in the presence of neutral acetic acid and −16 in the presence of acetate anion.

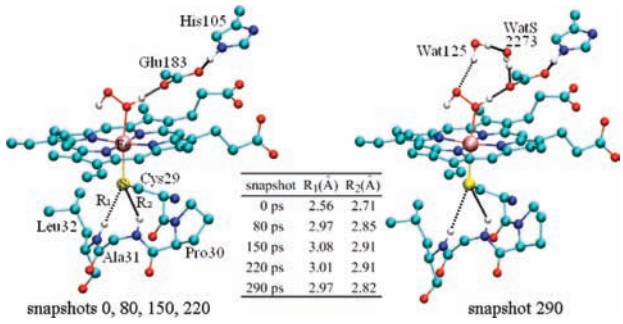

Figure 2. Hydrogen-bonding situations in CPO. Only hydrogen-bonded hydrogens are shown.

Substrate Models. To evaluate the effect of acetate as a substrate located at the substrate-binding site near Asn74, the presence of acetate as an anion (deprotonated) and acetic acid (protonated) as well as the absence of acetate was explored with Prot1 and Prot3. In the setup of the system with Prot1-2/Prot3, the substrate acetate was protonated/deprotonated, respectively.

2.3. Snapshots. To investigate the effect of different enzyme conformations on the stabilization of Cpd I, we performed a 300 ps force field MD simulation with a time step of 1 fs starting from the Fe−HOOH species with the residue protonation scheme of Prot1 and in the absence of acetate substrate. Then we selected four snapshots from the equilibrium trajectory, at 80, 150, 220, and 290 ps, which after MM energy minimizations were subsequently subjected to QM/MM geometry optimization. The 300 ps MD and subsequent MM energy minimization calculations were performed with the CHARMM22 force field[26] as implemented in the CHARMM program,[27] during which the coordinates of the heme, H_2O_2, the proximal ligand Cys29, the distal residues His105 and Glu183, and the outer 8 Å thick water of solvent layer were kept fixed.

Hydrogen Bonding Patterns. As shown in Figure 2, snapshot 0 (derived from the crystal structure) and all advanced snapshots reveal the existence of hydrogen bonds between the sulfur atom of Cys29 and the backbone NH groups of Ala31 and Leu32. In addition, in snapshot 290, one crystal water (Wat125) and one solvent water (WatS2273) molecule entered into the pocket and formed hydrogen bonds with the distal oxygen and carboxyl oxygen of Glu183, respectively. These two water molecules in snapshot 290 were admitted into the QM/MM optimization region.

Selenocysteine Mutant. The species of the selenocysteine mutant of CPO were generated, for protonation scheme Prot1 and in the absence of the acetate substrate, by replacing the Cys29 by selenocysteine in all five snapshots for WT CPO. The generated structures were subjected to QM/MM geometry optimization. The details of the force field parameters were described in our previous study.[22]

2.4. QM/MM Calculations. ***Software, Functional, and Geometry Optimization Methods.*** The QM/MM calculations were performed using ChemShell[28] interfaced with Turbomole[29] and DL_POLY.[30] The hybrid B3LYP functional[31−34] was used throughout this study for the QM part, and the CHARMM22 force field[26] was used for the MM part. An electronic embedding scheme[35] was applied to include the polarizing effect of the enzyme environment on the QM region. Hydrogen link atoms with the charge shift model[36] were used to treat the QM/MM boundary.

The optimized region considered in the QM/MM calculations is the same as our previous work[12] and involves Cys29/Se-Cys29, heme, H_2O_2, Ala27, Pro28, Pro30, Ala31, Leu32, Phe103, His105, Glu183, Phe186, Wat71, Wat330, and Wat332. For snapshot 290, Wat125 and WatS2273 were also included in the MM optimized region. The QM/MM geometry optimization used the HDLC optimizer[37] which is part of ChemShell. A rational function optimizer with the Powell update (P-RFO) for an explicit Hessian[37] was used for transition-state optimizations. The nature of the transition states (TS's) as first-order saddle points was confirmed by vibrational mode analysis based on the numerical calculation of a finite-difference Hessian for a selected set of QM atoms.

QM Models. Figure 3a specifies the three QM regions, QM1−3, which were investigated for the WT enzyme. They all included the iron porphine moiety, with its distal ligand (H_2O_2), and CH_3COO^- (representing Glu183) but differed in the representation of other residues. In QM1, as in the previous study,[12] the cysteine proximal ligand was modeled as the SH group, while His105 was modeled as a protonated imidazole. In QM2, the full Cys29 residue was included as well as part of the proximal loop that avoids cutting the QM system through the peptide bond, including the CO group of Pro28 and the pyrrolidine ring of Pro30. His105 was modeled by a protonated 5-methylimidazole in QM2. QM1 was used only in a snapshot 0 calculation, while the larger QM2 was used through all five snapshots that we studied in this paper. The last model in Figure 3a, labeled QM3, utilizes SH for Cys29, protonated 5-methylimidazole for His105, and the backbone of three amino acids that forms hydrogen bonds with the sulfur of Cys29 ($HCO-NHCH_2CO-NHCH_3$, i.e., the HCO group of Pro30, the $NHCH_2CO$ group of Ala31, and $NHCH_3$ of Leu32). This model was used only for the calculation of Mössbauer spectroscopic parameters. QM1, QM2, and QM3 consist of 60, 87, and 79 atoms, respectively. Figure 3b describes the QM model (Se-QM2) for the Se-Cys mutant in CPO. It corresponds to QM2 by replacing Cys29 with selenocysteine.

Basis Sets. QM/MM geometry optimization was performed using the standard double-ζ basis set B1, which involves LACVP on Fe and 6-31G on all other atoms except for Se in the CPO selenocysteine mutant system, hence LACVP(Fe): 6-31G(rest).[38,39] For the Se atom, the B1 basis set involves the double-ζ SV basis set of Binning and Curtiss.[40]

A basis set labeled B1a, which includes polarization and diffused functions on the three O atoms in the FeOOH···HOC(Glu183) moiety involved in the O−O bond cleavage, was utilized to get a better description of the O−O cleavage TS,[12] en route to the formation of Cpd I from Cpd 0.

In all cases, the energy was corrected by single point calculations with a larger basis set B2, which describes iron by Wachters's all electron basis set,[41] augmented with diffused d[42] and polarization f functions[43,44] (8s7p4d1f), and the rest of the atoms except Se in the CPO selenocysteine mutant system by the 6-31++G(d,p) basis set. For the Se atom, the B2 basis set augments B1 by a set of an s,p diffused function with an exponent of 0.022 and a polarization d function with an exponent of 0.315.[40] These single point calculations are labeled as B2//B1 or B2//B1a.

2.5. Calculations of Mössbauer Spectroscopic Parameters. The Mössbauer parameters of CPO Cpd I were calculated with the ORCA[45] program using a single-point B3LYP calculation at the corresponding QM/MM-optimized geometries at the B1 level. Iron was described by the triply polarized core properties basis set CP(PPP),[46] and the other atoms were described by the SV(P) basis set[47] with the inner s functions left uncontracted. For the iron atom, an enhanced integration grid was used, and the overall integration accuracy was increased to seven. The

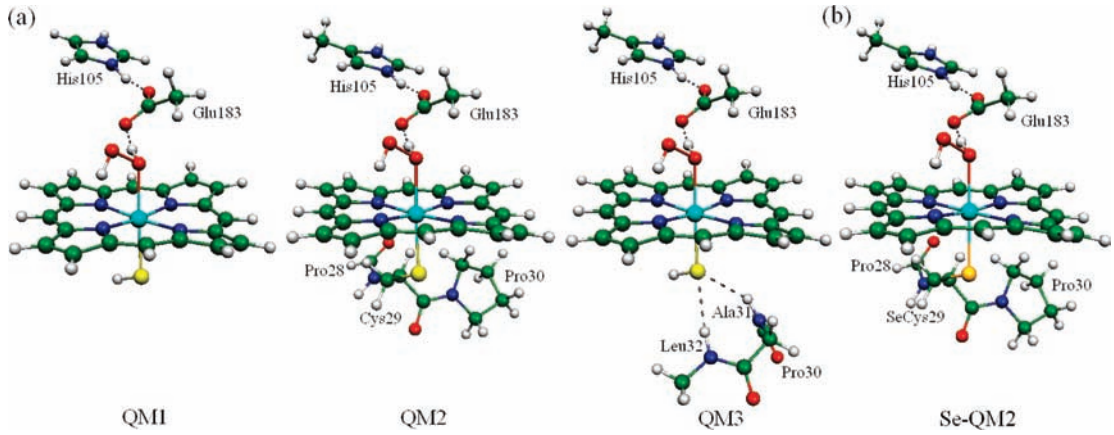

Figure 3. Definitions of the QM regions: (a) three QM models (QM1, QM2, and QM3) for the WT enzyme and (b) one QM model (Se-QM2) for the selenocysteine mutant (C29-SeC).

MM point charges were included in these calculations to probe the effect of the protein environment. The acetate was absent in all of the Mössbauer calculations in this study. Here, for snapshot 0, two QM regions (QM2 and QM3) as well as two protein protonation schemes (Prot1 and Prot3) were employed. The calculations were also performed without the water hydrogen-bonded to the iron−oxo moiety to ascertain its influence. For the other four snapshots and Se-Cys mutant, only QM2 and Prot1 were used.

3. Results

3.1. Relative Energies of Cpd I and Cpd 0. The energy of Cpd I relative to Cpd 0 can serve as an index of stability of Cpd I. The previous QM/MM calculations[12] on the Cpd I formation mechanism in CPO using Prot3 and QM1 showed that Cpd I is only 1.5 kcal/mol lower than Cpd 0 at the QM/MM B2 level. As already mentioned, this relative energy, compared with that from the QM/MM calculation on cytochrome P450cam,[13] does not explain why Cpd I of CPO can be probed in its native cycle, while that of P450cam is too short-lived to be detected in its native cycle. To address this issue, we extensively studied the effect of the following five factors on the relative Cpd 0/Cpd I energy: (1) substrate, (2) QM regions, (3) protonation states of residues, (4) protein conformations, and (5) proximal ligand mutation. Only the results at the B2 level are reported here. The rest of the data are collected in the Supporting Information document.

3.1.1. Effect of Substrate. To evaluate the effect of acetate as a substrate, three models (the presence of deprotonated and protonated acetate and the absence of acetate substrate) were used for snapshot 0. In our previous study,[12] the substrate acetate was modeled as a deprotonated species, while the protonation scheme of the rest of the enzyme and the QM region were limited to Prot3 and QM1, and optimization was done with the basis set B1a. For comparison, we studied here both protonation states, Prot1 and Prot3. For the sake of consistency, we used here the basis set B1 for geometry optimization throughout, while the relative energies were evaluated with B2.

The B2//B1 relative energies are shown in Figure 4. Figure 4a,b shows the effect of acetate protonation within Prot3/QM1 which represents the protonation scheme Prot3 and the QM region QM1. It is seen that protonation of the acetate favors Cpd I relative to Cpd 0 by 11.6 kcal/mol. In fact, as can be seen from Figure 4b, the removal of the protonated acetate almost does not change the relative energy. Moreover, as can

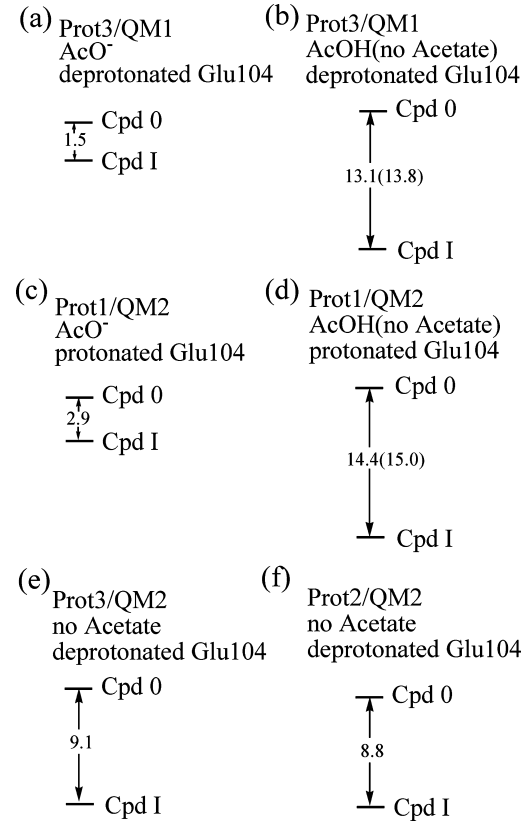

Figure 4. Relative energies (kcal/mol) of Cpd I to Cpd 0 for the snapshot 0 of WT CPO at the B2//B1 level. (a) Prot3/QM1 in the presence of AcO^-. (b) Prot3/QM1 in the presence of AcOH and in the absence of acetate (in parentheses). (c) Prot1/QM2 in the presence of AcO^-. (d) Prot1/QM2 in the presence of AcOH and in the absence of acetate (in parentheses). (e) Prot3/QM2 in the absence of acetate. (f) Prot2/QM2 in the absence of acetate.

be seen from Figure 4c,d, this conclusion is not dependent on the protonation state of the entire enzyme or on the chosen QM system.

These results indicate that the acetate anion significantly destabilizes Cpd I by unfavorable electrostatic interaction with the heme center. From our calculations of Prot1 in the absence of acetate in the substrate binding site or with protonated acetate, Cpd I is about 15.0 kcal/mol more stable than Cpd 0 (Figure 4d), which is in between the calculated values of 27 kcal/mol for horseradish peroxidase (HRP)[48,49] and of about 8−10 kcal/mol for P450cam (Asp251 channel).[13] Hence, without the

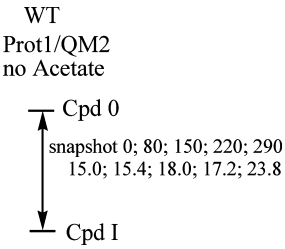

Figure 5. Energies (kcal/mol) of Cpd I relative to Cpd 0 for five snapshots of WT CPO using Prot1/QM2 in the absence of substrate acetate at the B2//B1 level.

destabilization effect of anion acetate substrate, the order of the relative energy of Cpd I in various heme enzymes is in accord with the experiment: HRP > CPO > P450. Therefore, we used the substrate-free model in the following studies.

3.1.2. Effect of QM Regions and Protonation States. The data in Figure 4e,f show the effect of the QM region and protonation schemes of specific residues on the relative Cpd 0/Cpd I energy (Prot3/QM2 and Prot2/QM2 in the absence of acetate). Comparison of Prot3/QM1 versus Prot3/QM2 in Figure 4b versus Figure 4e shows that increasing the QM system from QM1 to QM2 raises the relative energy of Cpd I by 4.7 kcal/mol, which is similar to the value in a previous QM/MM calculation of cytochrome P450cam.[13] Comparison of Figure 4e to Figure 4f shows, in turn, that changing from Prot3 to Prot2 (both having deprotonated Glu104) has a very small effect on the relative Cpd 0/Cpd I stability (0.3 kcal/mol). This result is similar to our previous QM/MM calculation,[12] which used a neutral protonation scheme in which acetate and Glu104 were both deprotonated. Finally, comparison of Figure 4f to Figure 4d shows that the protonation of Glu104 favors the Cpd I relative to Cpd 0 by 6.2 kcal/mol.

In summary, all of the above results indicate that the most important factors to affect the Cpd I relative energy to Cpd 0 are the protonation states of substrate acetate and Glu104.

3.1.3. Effect of Protein Conformation. To probe the influence of different conformations of the enzyme environment on energetic stabilization, we compared the QM/MM energies of Cpd I relative to Cpd 0 for the five selected snapshots for the acetate substrate-free model with Prot1/QM2. The data displayed in Figure 5 show that Cpd I is favored in all snapshots. With the exception of snapshot 290, the Cpd 0/Cpd I relative energy value is 16.5 ± 1.5 kcal/mol, thus exhibiting a small dependence on the protein environment. For snapshot 290, in which two additional water molecules entered the pocket (Figure 2), Cpd I is significantly more stable than Cpd 0. Inspection of the relative energy of Cpd 0 to the Fe−HOOH species (Table S4 in the Supporting Information) revealed that, for snapshot 290, this relative energy is 6.7−11.4 kcal/mol higher than for the other four snapshots, whereas at the same time, the energy of Cpd I relative to Fe−HOOH is within a range of 3.1 kcal/mol for all five snapshots. As such, it seems that the root cause of the large Cpd 0/Cpd I relative energy in snapshot 290 is the destabilization of Cpd 0 by the two water molecules. As shown below this destabilization has a geometric origin.

3.1.4. Geometric and Electronic Features. Figure 6a,b shows geometrical parameters and spin densities for the QM/MM optimized structures derived from the five snapshots for the WT enzyme. It can be seen from Figure 6a that the Fe−N distances show a minor variation for all three species: Fe−HOOH, Cpd 0, and Cpd I. The Fe−O distances of Fe−HOOH and Cpd 0 were found to be more flexible. The longest bond was found for snapshot 290 in which one water molecule (Wat125) forms a hydrogen bond (H-bond) with the distal oxygen of the FeHOOH/FeOOH moiety. This H-bond pulls the Fe−OO unit and causes the lengthening of Fe−O by 0.02−0.04 Å. The weakened Fe−O bond destabilizes Cpd 0 and results in a higher relative energy of Cpd 0 to Cpd I. In addition, the Fe−S distances of Cpd 0 and Cpd I exhibit some fluctuation similar to a previous finding in P450 Cpd I.[50]

The spin densities in Figure 6b are what one expects from these species.[51] The sulfur spin density in Cpd I is close to that of previous studies of P450 Cpd I[50] and to the experimental datum from ENDOR spectroscopy of CPO Cpd I.[5]

3.1.5. Effect of Selenocysteine Mutation. The relative energies of Se−Cpd 0/Se−Cpd I, for the selenocysteine mutant, are shown in Figure 7 for all of the snapshots and Prot1/QM2. It is seen that these relative energies are very similar to those of the WT enzyme in Figure 5, to within 1 kcal/mol. Apparently, the mutation of cysteine to selenocysteine has little if any effect on the relative Cpd 0/Cpd I stability, even though one might have reasoned that the effect should be considerable since the selenocysteine ligand has a stronger push effect compared with the cysteine ligand.[22]

The geometric parameters and spin densities for the selenocysteine mutant are given in Figure 8a,b. Inspection of Figure 8a reveals that the calculated Fe−Se bonds of ferric hydrogen peroxide (Se−Fe−HOOH), Se−Cpd 0, and Se−Cpd I are about 0.08 Å longer than the Fe−S bonds of the corresponding WT species (Figure 6a), while other key geometric parameters are very similar for the WT species and selenocysteine mutants. By contrast, in the case of P450cam Cpd I,[22] the QM/MM result showed that the Fe−Se bond is significantly longer than Fe−S by 0.18 Å. In fact, inspection of Figure 8b shows that the Se spin density of Se−Cpd I is almost identical to that in the WT Cpd I (Figure 6b). Again, this is in contrast to the results of P450cam, where the sulfur spin density, 0.25, was much smaller than the selenium spin density, 0.40.[22] Apparently, the polar pocket of CPO stabilizes the Cys-Se^- anionic form much more so than the P450cam pocket and thereby applies a leveling effect on the two ligands.

3.2. Mössbauer Spectroscopic Parameters. The calculated Mössbauer parameters of the WT Cpd I of snapshot 0 with Prot1/Prot3 and QM2/QM3 are collected in Table 1, while those of the WT and Se−Cpd I of all snapshots with Prot1/QM2 are in Table 2. The calculated quadrupole splitting (ΔE_Q) and isomer shifts (δ) parameters in Table 1 are in reasonably good accord with experimentally observed Mössbauer parameters for CPO S−Cpd I (last entry in Table 1). The values for QM3 are closest to the experimental values, as found in a previous study,[52] using a different basis set for geometry optimization. Within the results for Prot1, the QM2 values are slightly better than those of QM3. It is clear that removing the water molecule, which is liberated during the process of Cpd I formation from Cpd 0, results in a slightly lower ΔE_Q, which deviates from the experimental value.

Table 2 compares the Mössbauer parameters of S−Cpd I and Se−Cpd I for the five snapshots derived from Prot1/QM2. Once again, it is apparent that Se−Cpd I is very similar to the WT Cpd I in CPO. This is again in contrast to P450cam (see last entry), where the Se−Cpd I was calculated to have Mössbauer parameters more akin to a gas-phase species with a large radical on the chalcogen ligand (spin density (Se) = 0.40). The different pocket polarities seem to play a major role: In P450cam with the nonpolar pocket, the selenolate anion is not stabilized, and the WT Cpd I differs considerably with relation to Se−Cpd I. On the other hand, in CPO with the polar pocket, there is a

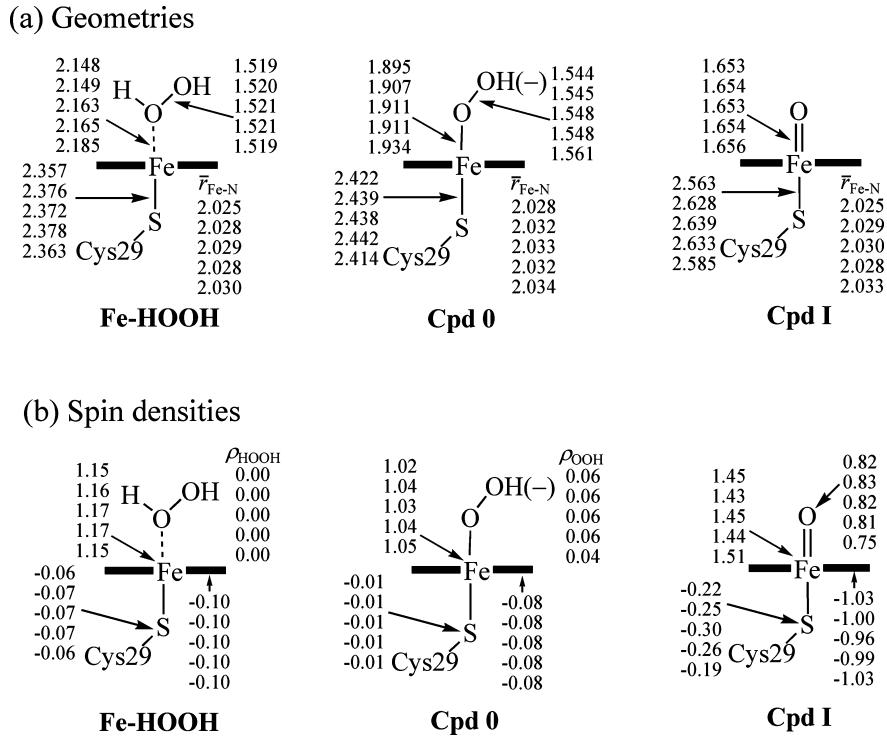

Figure 6. QM/MM optimized (a) geometries and (b) spin densities of Fe−HOOH, Cpd 0, and Cpd I of the WT enzyme. The given values correspond to snapshots 0, 80, 150, 220, and 290 in descending order.

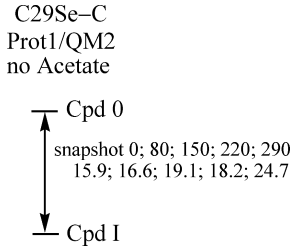

Figure 7. Energies (kcal/mol) of Se−Cpd I relative to Se−Cpd 0 for five snapshots of C29Se−C using Prot1/QM2 in the absence of substrate acetate at the B2//B1 level.

leveling effect, and the two Cpd I species are virtually indistinguishable.

3.3. Barriers for Cpd I Formation from Cpd 0. Since our previous study[12] indicated that the rate-limiting step of the formation of Cpd I in CPO is the O−O bond breaking step, we limited the study here to this step. A model with Prot1/QM2 in the absence of acetate was used for snapshot 0. At the QM/MM B2//B1a level, the barrier of O−O cleavage from Cpd 0 to generate Cpd I is 10.1 kcal/mol, passing via the familiar homolytic/heterolytic hybrid TS. This barrier is smaller than the one calculated (12.4 kcal/mol) in the previous study[12] using Prot3/QM1 in the presence of the acetate anion. As shown in Figure 9a, in the absence of acetate, the O−O bond distance (1.783 Å) in the TS structure S-$\mathbf{TS}_{OO}$ is shorter than the previous value (1.816 Å), indicating an earlier TS with a lower energy. We noticed that, for the corresponding step in P450cam, the QM/MM estimation of a barrier with a similar QM region and computational level is larger by about 4−5 kcal/mol than the one obtained here.

Interestingly, the corresponding barrier for Se−Cpd I formation in the selenocysteine mutant is also 10.0 kcal/mol, namely, the same as for WT CPO. As shown in Figure 9b, the TS structure (Se-$\mathbf{TS}_{OO}$) is indeed very similar to the WT one (S-$\mathbf{TS}_{OO}$). The O−O bond distance is 1.781 Å in Se-$\mathbf{TS}_{OO}$ compared with 1.783 Å in S-$\mathbf{TS}_{OO}$. Thus, once again we witness that within the CPO pocket the "push" effect of the selenocysteine ligand is not expressed, and Se−Cpd I is predicted to be formed at the same rate as the S−Cpd I and be as stable. Since S−Cpd I is observable, so must be Se−Cpd I!

4. Discussion

The above results reveal two major trends: (a) the presence of an anionic or neutral substrate (like acetate and acetic acid) and the protonation state of Glu104 have a considerable effect on the stability of Cpd I relative to Cpd 0; the anionic substrate also raises the barrier for Cpd I formation. (b) The mutation of the proximal ligand from cysteine to selenocysteine has little or no effect on the stability of Cpd I and its rate of formation. We shall now discuss these features in turn.

4.1. Role of Anionic Substrate and Glu104. As argued in Section 3.1.1, the interaction between the acetate and the heme center is mainly of classical electrostatic character (recall the acetate is in the MM region). So we can view deprotonated acetate as a negative point charge and consider its charge−dipole interaction energy with the QM system, using the following expression:

$$V = Q\vec{R}\cdot\vec{\mu}/|\vec{R}|^3 \qquad (1)$$

Here, Q is the point charge, and $\vec{\mu}$ is the heme dipole moment vector; $\vec{R}$ is the vector from the center of the dipole to point charge. Since eq 1 has an inner product of $\vec{R}$ and $\vec{\mu}$, the dipole components perpendicular to the vector $\vec{R}$ will have no contribution to the charge−dipole interaction.

Figure 10 shows the heme, acetate, and Glu104 in a Cartesian coordinate system, where z is oriented along the FeO bond and x and y lie in the demi-plane defined by the two nitrogen atoms of the porphine. It is seen that a positive dipole along the z-axis is defined from a negative to a positive charge along the z-axis.

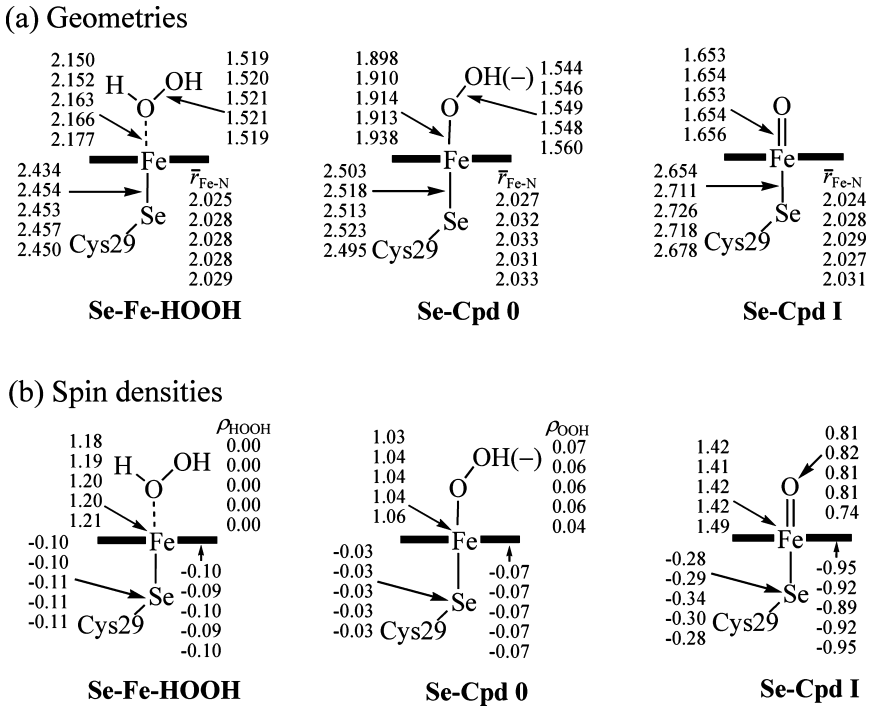

Figure 8. QM/MM optimized (a) geometries and (b) spin densities of Se−Fe−HOOH, Se−Cpd 0, and Se−Cpd I of selenocysteine mutants. The values correspond to snapshots 0, 80, 150, 220, and 290 in descending order.

TABLE 1: Calculated Mössbauer Parameters for S−Cpd I of CPO

			ΔE_Q (mm/s)	δ (mm/s)	η
water	QM2	Prot1	0.92	0.12	0.29
		Prot3	0.83	0.12	0.41
	QM3	Prot1	0.87	0.13	0.29
		Prot3	0.95	0.12	0.26
without water	QM2	Prot1	0.89	0.13	0.30
		Prot3	0.81	0.14	0.32
	QM3	Prot1	0.84	0.13	0.30
		Prot3	0.88	0.14	0.27
		exp[a]	1.02	0.15	n/a

[a] Value from ref 3.

Since acetate lies very near to the z-axis, it will stabilize any species with a positive dipole in proportion to the size of the μ_z dipole component.

Table 3 shows the calculated dipole moments of the QM system with the MM point charges included, for Prot3/QM1 and Prot1/QM2 in the Cartesian coordinate system defined in Figure 10. It can be seen that the μ_z component of the heme dipole is positive for both Cpd 0 and Cpd I and is larger for Cpd 0. As such, the charge−dipole interaction with acetate will stabilize both species but be more stabilizing for Cpd 0 and thereby impact the relative Cpd 0/Cpd I stability. Accordingly, in the absence of acetate anion, or when acetate is protonated, the exothermicity of the Cpd I formation is significant, −13.8 (−15.0) kcal/mol. By contrast, in the presence of acetate, the reaction is almost thermoneutral, and Cpd I is only 1.5 (2.9) kcal/mol more stable than Cpd 0, for Port3/QM1 (Prot1/QM2).

The above rationale, based on eq 1, explains also the effect of protonation/deprotonation of Glu104 on the stabilization of Cpd I relative to Cpd 0. Thus, as can be seen from Figure 10, Glu104 lies near the positive x-axis, and therefore, the dominant charge−dipole interaction term will involve the x-component of the heme dipole moment. As the CPO species changes from Cpd 0 to Cpd I, the x-dipole component in Table 3 decreases, and therefore the deprotonated Glu104 will stabilize Cpd 0 relative to Cpd I, whereas a protonated Glu104 will not have this favorable interaction with Cpd 0. Indeed, as can be seen in Figure 4d versus Figure 4f, when Glu104 is protonated, the exothermicity of Cpd I formation is −15.0 (for Prot1/QM2), whereas with deprotonated Glu104, the exothermicity is only −8.8 kcal/mol (for Prot2/QM2).

It appears therefore that the working pH of CPO will affect its activity markedly. A basic pH will prefer deprotonated Glu104 and acetate, decrease the exothermicity of Cpd I formation, and increase the corresponding barrier. By contrast, an acidic pH will increase the stability of Cpd I and lower the barrier to its formation. As can be seen from the TS structures in Figure 9, this is a simple Hammond effect; Cpd I becomes more stable and the TS leading to it earlier and lower in energy. It is interesting to note that the optimum pH of CPO is 2.85 for chlorination.[53]

4.2. Effect of Proximal Ligand Mutation. The above results indicate that selenocysteine mutation of CPO has almost no effect on the formation of Cpd I. This is different from the case of P450 in which Se−Cpd I was found to have different geometry and a different spin density from S−Cpd I. Thus, in P450cam, the spin density on Se was calculated to be almost twice as large as that on S, and the Fe−Se bond was significantly longer than Fe−S.[22] By contrast, in CPO, the Se and S spin densities are nearly identical, and the Fe−Se and Fe−S bonds are not very different in length; the Cpd 0/Cpd I relative stability as well as the barriers for Cpd I formation are virtually identical for the WT and the mutant. As we already noted, these different findings are rooted in the pocket polarities of P450cam versus CPO. The pocket of CPO is polar, and therefore it stabilizes the anionic form of the proximal ligand (Cys-S$^-$ and Cys-Se$^-$) relative to the radical form (Cys-S$^\bullet$ and Cys-Se$^\bullet$). The pocket polarity is evidently sufficiently large to exert a leveling effect and render the two ligands almost identical. By contrast, the

TABLE 2: Calculated Mössbauer Parameters for S−Cpd I and Se−Cpd I for Five Snapshots Generated for QM2/Prot1

		S−Cpd I			Se−Cpd I		
		ΔE_Q (mm/s)	δ (mm/s)	η	ΔE_Q (mm/s)	δ (mm/s)	η
CPO	snapshot 0	0.92	0.12	0.29	1.01	0.12	0.25
	snapshot 80	1.09	0.13	0.15	1.11	0.13	0.14
	snapshot 150	1.15	0.13	0.12	1.18	0.12	0.10
	snapshot 220	1.11	0.13	0.13	1.14	0.12	0.12
	snapshot 290	1.14	0.12	0.12	1.03	0.12	0.20
P450cam[a]	snapshot 2	1.00	0.12	0.02	0.67	0.13	0.09

[a] Snapshot 2 (40 ps) of P450cam in the doublet state from ref 22.

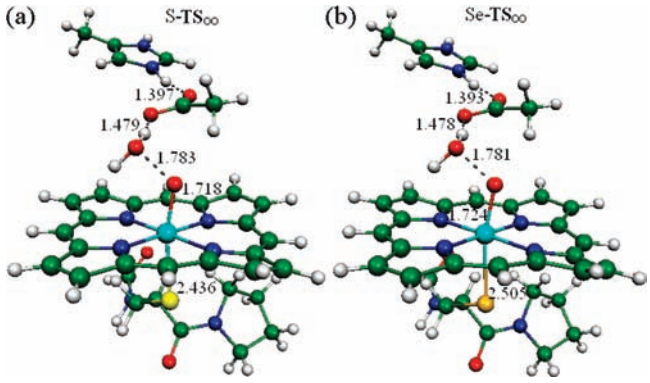

Figure 9. Structures of the TS of Cpd I formation from Cpd 0, for (a) S-**TS**$_{OO}$ and (b) Se-**TS**$_{OO}$.

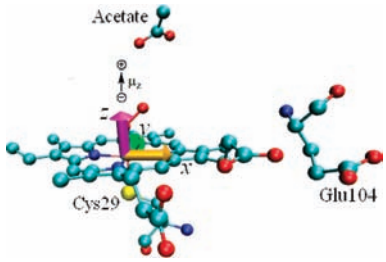

Figure 10. Heme center in the coordinate axes system, the substrate acetate, and Glu104. Shown also is the convention for a positive z-component of the dipole moment.

TABLE 3: Calculated Dipole Moment Components (in Atomic Units) for Various CPO Species[a,b]

	Prot3/QM1			Prot1/QM2		
	μ_x	μ_y	μ_z	μ_x	μ_y	μ_z
S−HOOH	5.57	−0.42	8.21	4.63	−4.21	7.63
S−Cpd 0	8.70	−0.12	11.11	7.57	−4.78	9.53
S−Cpd I	−2.86	0.02	6.28	3.37	−3.76	3.07

[a] All μ calculations are in the absence of substrate acetate. [b] The QM system is calculated with the B2 basis set, and all MM charges are included.

P450cam pocket is less polar, and therefore the selenocysteine ligand donates more electron density to the porphyrin cation radical and acquires a larger radical character. This difference in pocket polarities is reminiscent of the leveling effect of water on acidities compared with the intrinsic acidities in the gas phase.

This difference is in line with the role of proximal ligand in these two enzymes. In P450, the ability of the axial ligand to donate electrons to the iron−porphyrin, that is, the push effect, has been implicated to have a significant impact on the O−O bond cleavage and the formation of Cpd I from Cpd 0.[54,55] By contrast, in CPO, the role of the proximal ligand has been examined before by the replacement of the axial cysteine residue with a histidine, and the results indicated that the nature of the axial ligand in CPO does not affect the enzymatic activities.[56] Thus, CPO poses a unique opportunity for making Se−Cpd I and observing it.

5. Conclusions

The effects of the anionic substrate, protein environment, and proximal ligand mutation on the high-valent iron−oxo species, Cpd I, and the ferric hydroperoxide complex, Cpd 0, of CPO reveal a few intriguing trends. Thus, in the absence of the substrate or when it is protonated, Cpd I is considerably more stable, and its formation barrier is smaller compared with the case where the substrate is in its anionic state and when Glu104 is deprotonated. This trend, which is shown to be a simple manifestation of the Hammond principle, reproduces the experimental observation that the working pH of the enzyme is acidic. Furthermore, for a protonated substrate (or in its absence), the relative Cpd 0/Cpd I energy is found to be a good index of Cpd I stability in heme enzymes, thereby reproducing the experimental stability order: HRP > CPO > P450.

In silico mutation of the proximal ligand from cysteine to selenocysteine was found to exert no effect at all on the properties of Cpd I (e.g., spin density on the chalcogen, Mössbauer parameters, etc.) and its relative stability to Cpd 0 or on the corresponding barrier for formation. This is unlike the case of P450cam where Se−Cpd I was found to be very different from S−Cpd I, having a considerably long Fe−Se bond, a large Se-spin density, and Mössbauer parameters akin to a gas-phase species, in contrast to S−Cpd I with the relatively short Fe−S bond, small S-spin density, and very different Mössbauer parameters. This intriguing difference highlights the impact of the protein environment on the chameleonic Cpd I species.[57−59] Thus, the polar CPO pocket applies a leveling effect that stabilizes the anionic forms of both proximal ligands ($CysS^-$ and $CysSe^-$) to an extent that diminishes the radical characters ($CysS^\bullet$ and $CysSe^\bullet$). On the other hand, within the relatively nonpolar pocket of P450, the more reducing selenocysteine ligand acquires a high radical character (spin density of 0.40) by donating more electron density to the porphyrin cationic radical macrocycle.

The leveling effect in CPO means in turn that the Se−Cpd I of the mutant is observable. This poses a unique opportunity for making Se−Cpd I, observing it, and perhaps using it to learn how to make the corresponding species in P450.

Acknowledgment. S.S. is supported by the ISF (Grant 16/06). H.C. thanks the Golda Meir fellowship fund.

Supporting Information Available: Full set of computational results. This material is available free of charge via the Internet at http://pubs.acs.org.

References and Notes

(1) Dawson, J. H.; Sono, M. *Chem. Rev.* **1987**, *87*, 1255.
(2) Manoj, K. M.; Hager, L. P. *Biochemistry* **2008**, *47*, 2997.
(3) Rutter, R.; Hager, L. P.; Dhonau, H.; Hendrich, M.; Valentine, M.; Debrunner, P. *Biochemistry* **1984**, *23*, 6809.
(4) Hosten, C. M.; Sullivan, A. M.; Palaniappan, V.; Fitzgerald, M. M.; Terner, J. *J. Biol. Chem.* **1994**, *269*, 13966.
(5) Kim, S. H.; Perera, R.; Hager, L. P.; Dawson, J. H.; Hoffman, B. M. *J. Am. Chem. Soc.* **2006**, *128*, 5598.
(6) Sono, M.; Roach, M. P.; Coulter, E. D.; Dawson, J. H. *Chem. Rev.* **1996**, *96*, 2841.
(7) Denisov, I. G.; Makris, T. M.; Sligar, S. G.; Schlichting, I. *Chem. Rev.* **2005**, *105*, 2253.
(8) Yi, X. W.; Conesa, A.; Punt, P. J.; Hager, L. P. *J. Biol. Chem.* **2003**, *278*, 13855.
(9) Sundaramoorthy, M.; Terner, J.; Poulos, T. L. *Chem. Biol.* **1998**, *5*, 461.
(10) Poulos, T. L.; Kraut, J. *J. Biol. Chem.* **1980**, *255*, 8199.
(11) Filizola, M.; Loew, G. H. *J. Am. Chem. Soc.* **2000**, *122*, 3599.
(12) Chen, H.; Hirao, H.; Derat, E.; Schlichting, I.; Shaik, S. *J. Phys. Chem. B* **2008**, *112*, 9490.
(13) Zheng, J. J.; Wang, D. Q.; Thiel, W.; Shaik, S. *J. Am. Chem. Soc.* **2006**, *128*, 13204.
(14) Kühnel, K.; Derat, E.; Terner, J.; Shaik, S.; Schlichting, I. *Proc. Natl. Acad. Sci. U.S.A.* **2007**, *104*, 99.
(15) Kühnel, K.; Blankenfeldt, W.; Terner, J.; Schlichting, I. *J. Biol. Chem.* **2006**, *281*, 23990.
(16) Sligar, S. G.; Gunsalus, I. C. *Proc. Natl. Acad. Sci. U.S.A.* **1976**, *73*, 1078.
(17) Hu, S.; Kincaid, J. R. *J. Am. Chem. Soc.* **1991**, *113*, 9760.
(18) Unno, M.; Ishimori, K.; Ishimura, Y.; Morishima, I. *Biochemistry* **1994**, *33*, 9762.
(19) Schulze, H.; Ristau, O.; Jung, C. *Eur. J. Biochem.* **1994**, *224*, 1047.
(20) Sono, M.; Perera, R.; Jin, S.; Makris, T. M.; Sligar, S. G.; Bryson, T. A.; Dawson, J. H. *Arch. Biochem. Biophys.* **2005**, *436*, 40.
(21) (a) Davydov, R.; Perera, R.; Jin, S. X.; Yang, T.-C.; Bryson, T. A.; Sono, M.; Dawson, J. H.; Hoffman, B. M. *J. Am. Chem. Soc.* **2005**, *127*, 1403. (b) Kim, S. H.; Yang, T. C.; Perera, R.; Jin, S. X.; Bryson, T. A.; Sono, M.; Davydov, R.; Dawson, J. H.; Hoffman, B. M. *Dalton Trans.* **2005**, 3464.
(22) Cohen, S.; Kumar, D.; Shaik, S. *J. Am. Chem. Soc.* **2006**, *128*, 2649.
(23) Jiang, Y. Y.; Ortiz de Montellano, P. R. *Inorg. Chem.* **2008**, *47*, 3480.
(24) Li, H.; Robertson, A. D.; Jensen, J. H. *Proteins* **2005**, *61*, 704.
(25) Bas, D. C.; Rogers, D. M.; Jensen, J. H. *Proteins* **2008**, *73*, 765.
(26) MacKerell, A. D., Jr.; Bashford, D.; Bellott, M.; Dunbrack, R. L., Jr.; Evanseck, J. D.; Field, M. J.; Fischer, S.; Gao, J.; Guo, H.; Ha, S.; Joseph-McCarthy, D.; Kuchnir, L.; Kuczera, K.; Lau, F. T. K.; Mattos, C.; Michnick, S.; Ngo, T.; Nguyen, D. T.; Prodhom, B.; Reiher, W. E., III; Roux, B.; Schlenkrich, M.; Smith, J. C.; Stote, R.; Straub, J.; Watanabe, M.; Wiórkiewicz-Kuczera, J.; Yin, D.; Karplus, M. *J. Phys. Chem. B* **1998**, *102*, 3586.
(27) Brooks, B. R.; Bruccoleri, R. E.; Olafson, B. D.; States, D. J.; Swaminathan, S.; Karplus, M. *J. Comput. Chem.* **1983**, *4*, 187.
(28) Sherwood, P.; de Vries, A. H.; Guest, M. F.; Schreckenbach, G.; Catlow, C. R. A.; French, S. A.; Sokol, A. A.; Bromley, S. T.; Thiel, W.; Turner, A. J.; Billeter, S.; Terstegen, F.; Thiel, S.; Kendrick, J.; Rogers, S. C.; Casci, J.; Watson, M.; King, F.; Karlsen, E.; Sjøvoll, M.; Fahmi, A.; Schäfer, A.; Lennartz, C. *J. Mol. Struct.: THEOCHEM* **2003**, *632*, 1.
(29) Ahlrichs, R.; Bär, M.; Häser, M.; Horn, H.; Kölmel, C. *Chem. Phys. Lett.* **1989**, *162*, 165.
(30) Smith, W.; Forester, T. R. *J. Mol. Graph.* **1996**, *14*, 136.
(31) Becke, A. D. *Phys. Rev. A* **1988**, *38*, 3098.
(32) Lee, C.; Yang, W. T.; Parr, R. G. *Phys. Rev. B* **1988**, *37*, 785.
(33) Becke, A. D. *J. Chem. Phys.* **1993**, *98*, 5648.
(34) Becke, A. D. *J. Chem. Phys.* **1993**, *98*, 1372.
(35) Bakowies, D.; Thiel, W. *J. Phys. Chem.* **1996**, *100*, 10580.
(36) de Vries, A. H.; Sherwood, P.; Collins, S. J.; Rigby, A. M.; Rigutto, M.; Kramer, G. J. *J. Phys. Chem. B* **1999**, *103*, 6133.
(37) Billeter, S. R.; Turner, A. J.; Thiel, W. *Phys. Chem. Chem. Phys.* **2000**, *2*, 2177.
(38) Hay, P. J.; Wadt, W. R. *J. Chem. Phys.* **1985**, *82*, 299.
(39) Friesner, R. A.; Murphy, R. B.; Beachy, M. D.; Ringnalda, M. N.; Pollard, W. T.; Dunietz, B. D.; Cao, Y. X. *J. Phys. Chem. A* **1999**, *103*, 1913.
(40) Binning, R. C., Jr.; Curtiss, L. A. *J. Comput. Chem.* **1990**, *11*, 1206.
(41) Wachters, A. J. H. *J. Chem. Phys.* **1970**, *52*, 1033.
(42) Hay, P. J. *J. Chem. Phys.* **1977**, *66*, 4377.
(43) Bauschlicher, C. W., Jr.; Langhoff, S. R.; Partridge, H.; Barnes, L. A. *J. Chem. Phys.* **1989**, *91*, 2399.
(44) Stewart, R. F. *J. Chem. Phys.* **1970**, *52*, 431.
(45) Neese, F. *ORCA*, Version 2.6, Revision 35; University of Bonn: Bonn, Germany, 2006.
(46) Neese, F. *Inorg. Chim. Acta* **2002**, *337*, 181.
(47) Schäfer, A.; Horn, H.; Ahlrichs, R. *J. Chem. Phys.* **1992**, *97*, 2571.
(48) Derat, E.; Shaik, S. *J. Phys. Chem. B* **2006**, *110*, 10526.
(49) Derat, E.; Shaik, S.; Rovira, C.; Vidossich, P.; Alfonso-Prieto, M. *J. Am. Chem. Soc.* **2007**, *129*, 6346.
(50) Schöneboom, J. C.; Lin, H.; Reuter, N.; Thiel, W.; Cohen, S.; Ogliaro, F.; Shaik, S. *J. Am. Chem. Soc.* **2002**, *124*, 8142.
(51) Shaik, S.; Kumar, D.; de Visser, S. P.; Altun, A.; Thiel, W. *Chem. Rev.* **2005**, *105*, 2279.
(52) Cho, K.-B.; Hirao, H.; Chen, H.; Carvajal, M. A.; Cohen, S.; Derat, E.; Thiel, W.; Shaik, S. *J. Phys. Chem. A* **2008**, *112*, 13128.
(53) Beckwith, J. R.; Hager, L. P. *J. Biol. Chem.* **1963**, *238*, 3091.
(54) Dawson, J. H. *Science* **1988**, *240*, 433.
(55) Yoshioka, S.; Takahashi, S.; Ishimori, K.; Morishima, I. *J. Inorg. Biochem.* **2000**, *81*, 141.
(56) Yi, X. W.; Mroczko, M.; Manoj, K. M.; Wang, X. T.; Hager, L. P. *Proc. Natl. Acad. Sci. U.S.A.* **1999**, *96*, 12412.
(57) Ogliaro, F.; de Visser, S. P.; Groves, J. T.; Shaik, S. *Angew. Chem., Int. Ed.* **2001**, *40*, 2874.
(58) de Visser, S. P.; Ogliaro, F.; Sharma, P. K.; Shaik, S. *Angew. Chem., Int. Ed.* **2002**, *41*, 1947.
(59) de Visser, S. P.; Shaik, S.; Sharma, P. K.; Kumar, D.; Thiel, W. *J. Am. Chem. Soc.* **2003**, *125*, 15779.

JP902898S